Carcinogenesis vol.30 no.5 pp.851–860, 2009
doi:10.1093/carcin/bgp052
Advance Access publication February 23, 2009

Interferon-α counteracts the angiogenic switch and reduces tumor cell proliferation in a spontaneous model of prostatic cancer

Luca Persano[1], Lidia Moserle[1], Giovanni Esposito[2], Vincenzo Bronte[2], Vito Barbieri[1], Massimo Iafrate[3], Marina P.Gardiman[4], Patrizia Larghero[5], Ulrich Pfeffer[5], Elisabeth Naschberger[6], Michael Stürzl[6], Stefano Indraccolo[2,*] and Alberto Amadori[1,2]

[1]Oncology Section, Department of Oncology and Surgical Sciences, University of Padova, Padova I-35128, Italy, [2]Istituto Oncologico Veneto-IRCCS, Padova I-35128, Italy, [3]Urology Section, Department of Oncology and Surgical Sciences, University of Padova, Padova I-35128, Italy, [4]Pathology Unit, Azienda Ospedaliera, Padova I-35128, Italy, [5]Functional Genomics, National Cancer Research Institute, Genova I-16132, Italy and [6]Department of Surgery, Division of Molecular and Experimental Surgery, Erlangen D-91054, Germany

*To whom correspondence should be addressed. Tel: +39 0498215875; Fax +30 0498072854;
Email: stefano.indraccolo@unipd.it

Interferon (IFN)-α is a cytokine with marked therapeutic activity in transplantable tumor models, that is in part due to angiogenesis inhibition. Aim of this study was to investigate the effects of IFN-α during the early phases of tumor development in the transgenic adenocarcinoma of the mouse prostate (TRAMP) model. To provide sustained IFN-α production, TRAMP mice were injected intraperitoneally with lentiviral vectors. IFN-α administration resulted in rapid and protracted upregulation of IFN-α-regulated genes associated with antiangiogenic and antiproliferative functions in the prostate of TRAMP mice, including guanylate-binding protein 1 (GBP-1), IFI204 and CXCL10-11. These transcriptional changes were accompanied by effects on the tumor vasculature, including significant reduction of intraductal microvessel density and increased pericyte coverage, and marked reduction of tumor cell proliferation, without induction of tumor necrosis. Intriguingly, GBP-1 and myxovirus resistance A, two IFN-regulated proteins, were found expressed in ∼40% of human prostate cancer samples analyzed, suggesting expression of endogenous IFN-α. Overall, these findings demonstrate that IFN-α is able to counteract the angiogenic switch and impairs tumor cell proliferation in preinvasive lesions. Since the angiogenic switch also marks progression of human prostatic cancer, these results highlight the potential of angiogenesis inhibitors for the development of chemoprevention strategies in high-risk individuals.

Introduction

Naturally-occurring inhibitors of angiogenesis include, among other factors, certain cytokines and chemokines that, in addition to their effects on cells of the immune system, regulate some critical endothelial cell (EC) functions (reviewed in ref. 1). Interferon (IFN)-α is the prototype of antiangiogenic cytokines and this activity was first noticed many years ago (2), and subsequently confirmed in different transplantable tumor models (3–5). The effects of IFN-α on the vasculature have been mainly attributed to inhibition of basic fibroblast growth factor (bFGF) production by tumor cells (6) or downregulation of interleukin-8 and vascular endothelial growth factor (VEGF) gene expression (7,8). Moreover, IFN-α has direct effects on EC, including impairment of their proliferation and migration (4,5). Recently, the gene expression profile induced by IFN-α in EC has been defined (9), and it was found that several genes encoding negative regulators of angiogenesis are upmodulated in EC, thus providing a potential amplification mechanism for this biological activity.

Class I IFNs have been shown to delay tumor growth in orthotopic (10,11) and transplantable prostatic cancer models (12,13). Relatively little is known about the biological activity of IFN-α during the early steps of tumorigenesis; a previous study, however, showed increased expression of IFN-γ and its receptors in basal cells of the normal prostate and in benign prostatic hyperplasia (14). We found it interesting to expand this limited knowledge by using the transgenic adenocarcinoma of the mouse prostate (TRAMP) model of prostatic cancer, a well-characterized transgenic model (15), in which an angiogenic switch has been shown to occur early during the course of the disease (16).

The angiogenic switch is a discrete event that can be triggered by various signals including genetic mutations, hypoxia and other metabolic stress, mechanical stress and the immune/inflammatory response, and it has been identified in several transgenic models of cancer (17). Importantly, in patients this event appears to occur at early stages of tumor progression, as indicated by studies of preinvasive lesions of prostatic (18) and breast cancer (19).

TRAMP mice express a SV40 T antigen (Tag) under control of the minimal rat probasin promoter and display mild to severe hyperplasia of the prostate epithelium, resembling prostatic intraepithelial neoplasia (PIN) by 6–12 weeks of age (15). The well-defined temporal and spatial pattern of tumor progression in TRAMP offers a unique window of opportunity for investigation of the effects of antiangiogenic agents during the earliest molecular events of the disease, as shown by several recent studies (20–22).

To determine IFN-α effects in this model, we delivered the *IFN-α* gene by using lentiviral vectors, as a means to provide low level but chronic release of the cytokine, and determined the transcriptional and morphologic changes associated with IFN-α expression in the prostate of TRAMP mice. Our findings indicate that inhibition of angiogenesis in preinvasive lesions is feasible and could represent a form of prophylaxis in patients at high risk of development of invasive prostatic cancer.

Abbreviations: bFGF, basic fibroblast growth factor; EC, endothelial cell; EGFP, enhanced green fluorescent protein; GBP-1, guanylate-binding protein 1; hGBP-1, human guanylate-binding protein 1; IFN, interferon; LV, lentiviral vectors; mAb, monoclonal antibody; MxA, myxovirus resistance A; PCR, polymerase chain reaction; PIN, prostatic intraepithelial neoplasia; TRAMP, transgenic adenocarcinoma of the mouse prostate; VEGF, vascular endothelial growth factor.

Materials and methods

Patients data

The 31 primary samples analyzed in this study for guanylate-binding protein 1 (GBP-1) and MxA expression (Table I) were obtained from newly diagnosed patients with prostatic cancer who underwent radical prostactectomy in the Urology Section of the Department of Oncology and Surgical Sciences. Informed consent was obtained from all the patients who entered this study. No patient referred history of reproductive or endocrine diseases. Hormonal therapy was received by only four patients (samples 3, 21, 25 and 30) for 1–3 months prior to surgery.

Animal handling and tissue preparation

TRAMP mice, a gift from N.M.Greenberg, were bred in our animal facilities under pathogen-free conditions. Animal care and treatments were conducted in accordance with established guidelines and protocols that comply with national and international laws and policies (European Economic Community Council Directive 86/609, OJ L 358, 12 December 1987). Six-weeks-old transgenic males were injected intraperitoneally with 1 μg of p24 equivalent of LV-enhanced green fluorescent protein (EGFP), LV-IFN or a LV lacking any insert (control); after reaching endpoint ages, portions of prostatic lobes were rapidly frozen on dry ice and stored at −80°C,or fixed in 4% formaldehyde and paraffin embedded.

Lentiviral vectors production

EGFP and murine IFN-α-encoding lentiviral vectors (LV-EGFP/LV-IFN) were generated by transfection of 293T cells as described previously (23).

Table I. Patterns of GBP-1 and MxA expression in human prostatic cancer

Sample	Age	Total prostate-specific antigen	Clinical stage	Gleason score	pT	GBP-1	MxA
1	61	7.02	T2a	7	pT3a	neg	pos[a]
2	58	7.28	T2a	9	pT3a	neg	n.d.
3	63	9.1	T2a	8	pT3b	neg	pos[a]
4	57	5	T2a	7	pT3a	neg	pos[a]
5	71	8.45	T2a	9	pT3b	neg	neg
6	61	7.2	T1c	7	pT3b	neg	neg
7	53	7	T1c	7	pT3a	neg	pos[b]
8	47	13.6	T1c	7	pT3a	neg	neg
9	59	4.7	T1c	5	pT2a	neg	neg
10	68	4.1	T1c	6	pT3a	neg	neg
11	61	2	T2a	7	pT3a	neg	neg
12	64	4.7	T1c	7	pT2c	neg	neg
13	65	18	T1c	6	pT2c	neg	n.d.
14	56	1.8	T1a	5	pT2c	neg	n.d.
15	71	3.69	T1b	7	pT3a	neg	neg
16	60	6.43	T1c	7	pT3a	neg	n.d.
17	71	18.1	T1c	8	pT3b	neg	n.d.
18	69	13.75	T1c	8	pT3a	neg	n.d.
19	62	47.5	T1c	9	pT3b	pos[b]	pos[a]
20	71	6.46	T2a	8	pT3a	pos[b]	neg
21	61	14.3	T1c	7	pT3b	pos[b]	pos[b]
22	51	18	T2b	7	pT3a	pos[b]	pos[b]
23	71	6.71	T2a	8	pT3a	pos[b]	n.d.
24	72	4.5	T2a	7	pT2c	pos[b]	pos[a]
25	70	6.8	T1c	0	pT3a	pos[a]	pos[a]
26	76	4	T2a	7	pT3a	pos[a]	neg
27	66	8.1	T1c	7	pT2c	pos[a]	pos[a]
28	64	35.2	T1c	7	pT3a	pos[a]	pos[b]
29	51	5.1	T2a	9	pT3a	pos[a]	pos[b]
30	54	10.9	T1c	7	pT3a	pos[a]	pos[a]
31	61	10.56	T1c	9	pT3b	pos[a]	pos[b]

Following immunohistochemistry analysis, GBP-1 expression was evaluated by two independent pathologists in a blinded fashion.
[a]Tumor and stroma GBP-1 expression; n.d., not done; neg, negative; pos, positive.
[b]Stromal GBP-1 expression.

The same vector devoid of the insert was used as a control. Lentiviral vectors were concentrated by ultracentrifugation in a Beckman centrifuge equipped with a SW41 rotor at 50 000*g* at 4°C for 2 h and resuspended in phosphate-buffered saline. The viral p24 antigen concentration was determined by human immunodeficiency virus-1 p24 enzyme-linked immunosorbent assay (Innogenetics, Gent, Belgium). Mice received 1 μg of vector p24, corresponding to 1×10^8 transducing units of the EGFP-encoding LV.

Vector biodistribution studies by real-time polymerase chain reaction

Evaluation of transduction efficiency was performed as described previously (23); briefly, genomic DNA was extracted from tumor cells or from various mouse tissues, using the Easy-DNA kit (Invitrogen, Carlsbad, CA). The EGFP copy number per microgram of genomic DNA was estimated in duplicate, using the EGFP734p real-time polymerase chain reaction (PCR) assay as previously reported (24). To quantify EGFP, a reference curve was prepared by amplifying serial dilutions of DNA extracted from a reference cell line, which contains one EGFP copy per cell; the computerized tomography values of the experimental samples were plotted against the reference curve and the EGFP copy number was then estimated. Appropriate negative controls were included in each experiment.

Reverse transcription–PCR and real-time PCR

Total RNA was isolated using the RNeasy mini kit (Qiagen, Hilden, Germany) according to manufacturer's instructions. Complementary DNA was synthesized from 0.5 to 1 μg of total RNA using Superscript II first-strand system for reverse transcription–PCR (Invitrogen). For real-time PCR analysis, the SYBR Green qPCR SuperMix-UDG (Invitrogen) dye and Gene AMP 5700 Sequence Detection System (PE Biosystems, Foster City, CA) were used according to manufacturer's instructions. Each sample was run in duplicate and experiments repeated at least three times. For all genes evaluated, transcript levels were normalized either to β-actin or glyceraldehyde-3-phosphate dehydrogenase, glucose-6-phosphate dehydrogenase and retinitis pigmentosa II messenger RNA levels. PCR efficiencies were always >95% and <105%. Primers used for PCR analysis are reported in supplementary Table I (available at *Carcinogenesis* Online).

Immunohistochemistry and immunofluorescence analysis

Four micrometer thick frozen or formalin-fixed paraffin-embedded tumor section was rehydrated and processed for immunohistochemistry by standard procedures. Tumor vessels were labeled with a rat anti-CD31 monoclonal antibody (mAb) (Becton-Dickinson, San Jose, CA); GBP-1 and MxA expression were determined by using the rat anti-human guanylate-binding protein 1 (hGBP-1) mAb 1B1 (25) and the mouse anti-MxA mAb M134 (26), respectively. Immunostaining was performed using the avidin–biotin–peroxidase complex technique (Vector Laboratories, Burlingame, CA) and 3-3′ diaminobenzidine (Dako, Glostrup, Denmark) as chromogen, and the sections were then lightly counterstained with Mayer's hematoxylin. Parallel negative controls obtained replacing primary antibodies with phosphate-buffered saline were run in all cases. Intraductal microvessel density was quantified by screening the CD31-stained sections for the areas of highest vascularity; 10 representative fields at magnification ×400 for each tumor were counted.

For immunofluorescence analysis, 4 μm thick frozen tumor sections were rehydrated and then incubated with a saturating solution consisting of 5% goat serum, 1% bovine serum albumin, 0.1% Triton X in phosphate-buffered saline. After saturation, slides were incubated with rabbit anti-Ki67 (Novocastra, Newcastle Upon Tyne, UK), anti-cleaved Caspase 3 (Cell Signaling Technologies, Danvers, MA), anti-IFI204 (27), mouse anti-MxA, rat anti-F4/80 (Invitrogen) or biotinylated anti-CD45 (Becton-Dickinson), washed and incubated with a goat anti-rabbit, anti-mouse or anti-rat Alexa Fluor 488/546 (Invitrogen) secondary antibody or streptavidin Alexa Fluor 488 (Invitrogen) secondary reagent. In a set of experiments, pericytes were stained with the rabbit anti-NG2 Ab (1:100 dilution; Millipore Corporation, Billerica, MA) and vessels with anti-CD31 mAb (Becton-Dickinson). To measure perfusion, mice were injected intravenously with 50 μl per mouse of dextran 70-fluorescein isothiocyanate (Invitrogen; stock solution 360 μM) 5 min prior to be killed. To identify hypoxic cells in the prostate of TRAMP mice, we used pimonidazole hydrochloride (Hypoxyprobe-1; Chemicon International, Temecula, CA) that was administered to mice intraperitoneally 1.5 h before killing at 100 mg/kg of body weight in saline.

Nuclei were stained with TO-PRO-3 iodide (1:1000 dilution; Invitrogen) for 15 min, before washing and mounting of coverslips on glass slides for microscopy. Confocal laser scanning microscopy was carried out with a Zeiss LSM 510 microscope (Zeiss, Jena, Germany) using argon (488 nm) and helium–neon (543–633 nm) laser sources. The number of fields analyzed varied between 4 and 8 per section, depending on tumor size; at least six sections for each treatment were analyzed. Images were collected at original magnification ×200. Quantification of $Ki67^+$ areas was carried out by calculating the percentage of the positive area in the entire tumor section by using Adobe Photoshop 6 software (Adobe Systems, San Jose, CA).

Statistical analysis

Results were expressed as mean value ± SD. Statistical analysis of data were performed using Student's *t*-test. To evaluate significant differences in the count of $Ki67^+$ areas and the correlation between GBP-1 and MxA immunohistochemistry results, Fisher's exact test was carried out and *P* value calculated. In all tests run, differences were considered statistically significant when $P < 0.05$ (two tail).

Results

Angiogenesis during tumorigenesis in the TRAMP model

To investigate the dynamics of vascular changes during tumorigenesis, TRAMP mice of different age and bearing tumors representative of the different steps of tumor progression were killed and their prostates analyzed to determine the intraductal microvessel density. As shown in Figure 1A, non-transgenic prostate lacked intraductal vessels; on the contrary, these vessels were found in early prostatic tumors, and their number increased in well-differentiated and poorly-differentiated carcinomas (Figure 1A). These morphological changes were accompanied by a stepwise increase in VEGF expression by week 8 of age, which marks the angiogenic switch in this tumor model (16), and a progressive increase in bFGF expression levels at later time points of analysis (Figure 1B).

We subsequently investigated the possible expression of endogenous IFN-α at various phases of disease progression. Results, shown in Figure 1C, indicate that several IFN-α-regulated transcripts,

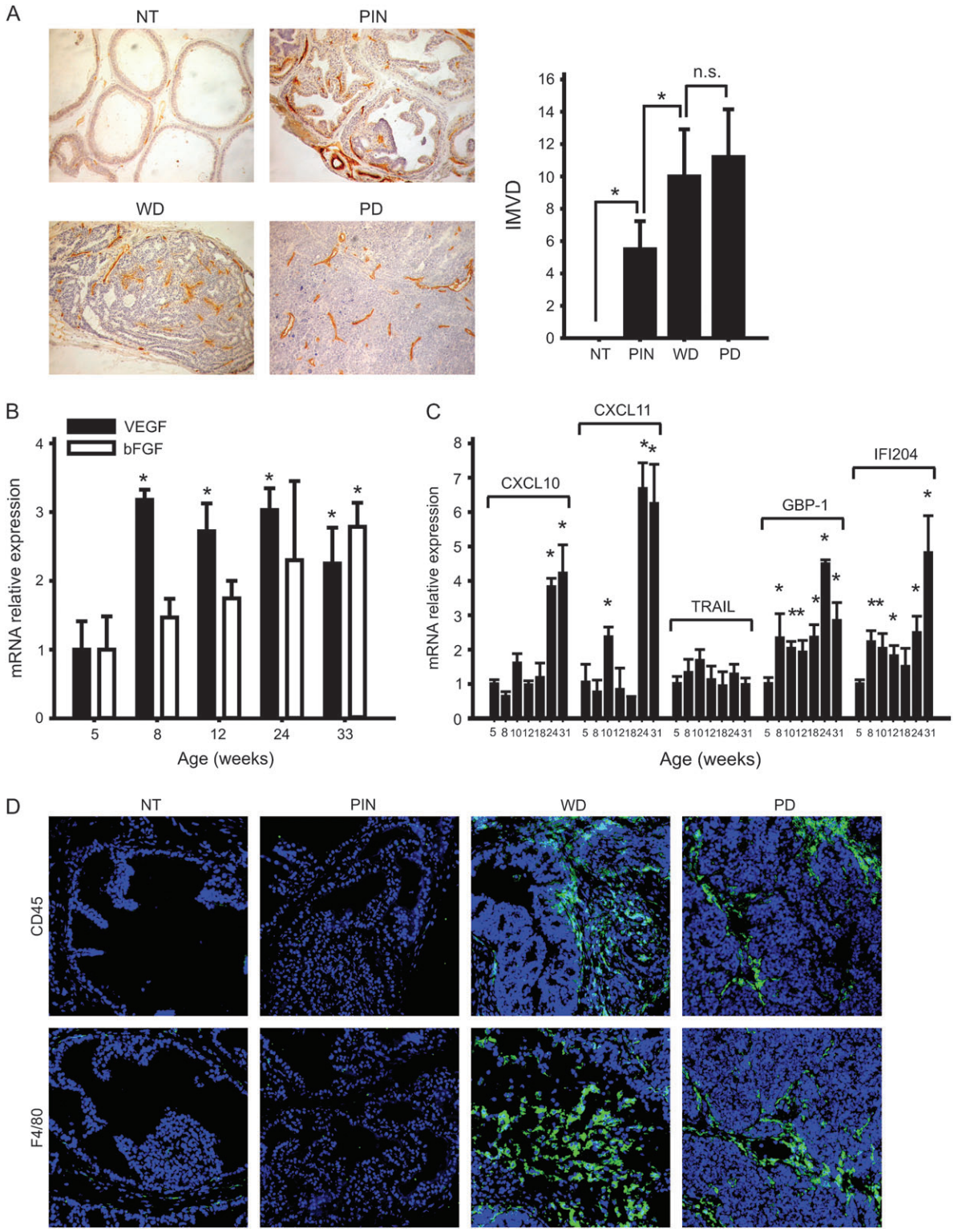

Fig. 1. Evaluation of angiogenesis during tumor progression in the TRAMP model. (**A**) Patterns of staining of microvessels and IMVD calculations. Left panel, prostates from non-transgenic C57BL/6 mice (NT) or TRAMP mice bearing PIN, well-differentiated (WD) and poorly-differentiated (PD) carcinoma were analyzed by CD31 immunohistochemistry (original magnification ×200). Right panel, intraductal microvessel density (IMVD) values at different stages of tumor progression. Four to six samples per each group were analyzed. Mean ± SD is shown. $^{*}P < 0.05$; n.s., not significant. (**B**) Relative expression of VEGF and bFGF was evaluated by quantitative PCR in the prostates of TRAMP mice of different age (from 5 to 33 weeks). Four samples per each group were analyzed. Mean ± SD is shown. $^{*}P < 0.05$. (**C**) Expression of IFN-α-regulated genes along tumor progression in TRAMP mice. Gene expression was analyzed by quantitative PCR in prostate samples obtained from TRAMP mice at the time points indicated. Three to five samples per each group were analyzed. Mean ± SD is shown. $^{*}P < 0.05$. (**D**) Evaluation of the inflammatory infiltrate of TRAMP tumors by CD45 and F4/80 staining (green). Representative pictures of PIN, WD and PD tumors or of NT prostate sample are shown (original magnification ×200).

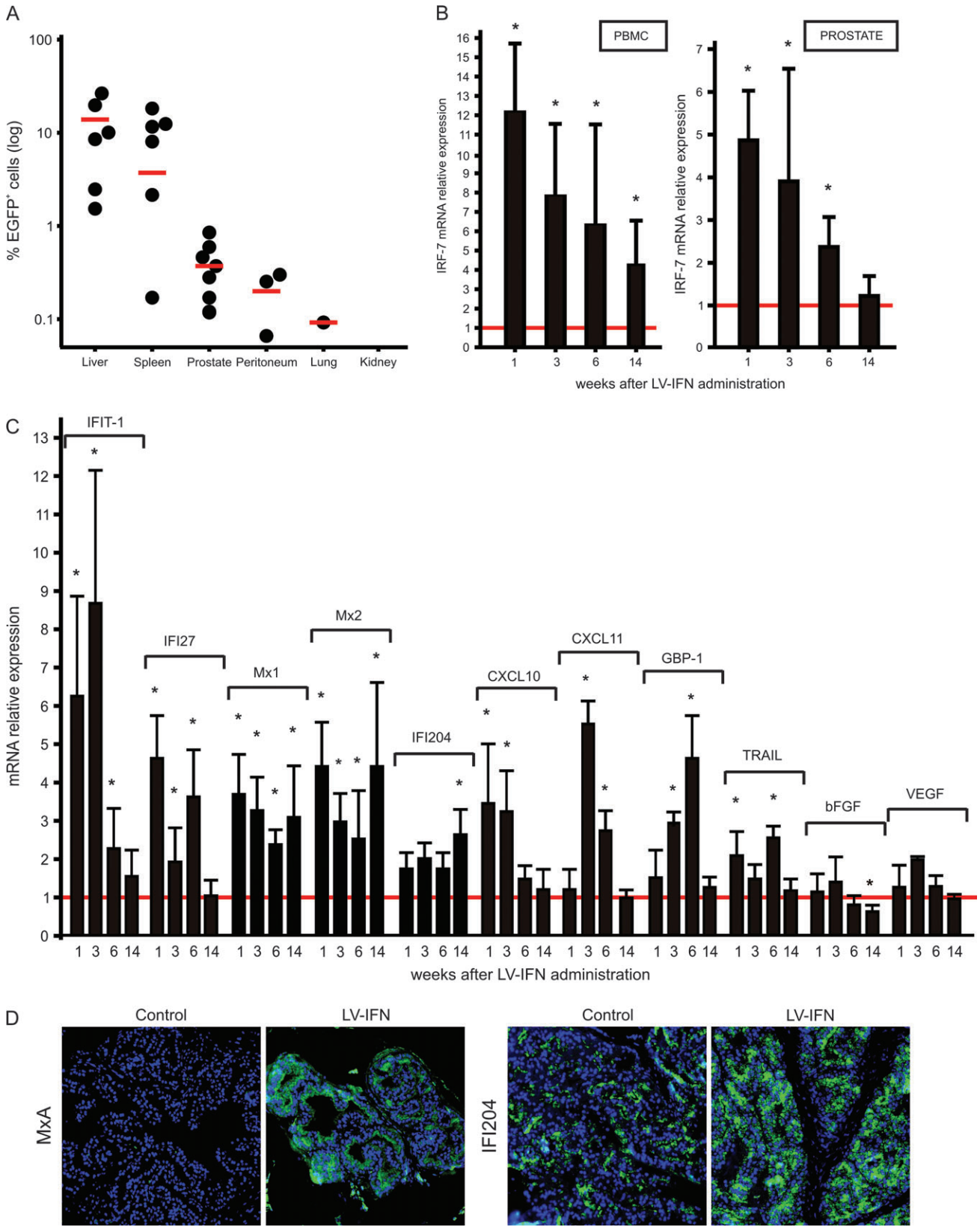

Fig. 2. Vector distribution studies and evidence of IFN-α transcriptional effects in TRAMP mice. Six-weeks-old TRAMP mice ($n = 6$) were injected intraperitoneally with EGFP- or IFN-α-encoding lentiviral vectors (LV-EGFP and LV-IFN, respectively; 1 μg p24 equivalent per mouse). Tissues from treated and control animals were analyzed by quantitative PCR at different time points. (**A**) Detection of vector sequences in TRAMP organs. The percentage of $EGFP^+$ cells was determined by quantitative PCR, 1 week after LV-EGFP injection. (**B**) Kinetics of mRNA IRF-7 expression in peripheral blood mononuclear cell (PBMC) (left panel) and prostate (right panel) from TRAMP mice were analyzed 1, 3, 6 and 14 weeks after LV-IFN injection. PBMC and portions of prostatic lobes were analyzed for the expression of IRF-7. Samples from TRAMP mice injected with the control vector were used as control (red line). Mean ± SD is shown. $^*P < 0.05$. (**C**) Expression of IFN-α-inducible transcripts in the prostate of TRAMP mice was analyzed 1, 3, 6 and 14 weeks after LV-IFN injection. The prostate from

including CXCL-10, CXCL-11, GBP-1 and IFI204 are initially found expressed at low levels and their levels rise with tumor progression. Interestingly, leucocyte and macrophage infiltration dramatically increased in advanced tumor stages compared with the initial lesions (Figure 1D); production of endogenous IFNs by these inflammatory cells could possibly explain the detection of IFN-regulated genes in the late stages of the disease.

Evidence of gene transfer in vivo and evaluation of IFN-α-mediated biological effects

Initially, TRAMP mice received an EGFP-coding lentiviral vector and vector biodistribution was investigated by quantitative PCR. As shown in Figure 2A, vector DNA sequences were detected mainly in the liver and the spleen of injected mice (range: 1.47–26.43% and 0.17–18.18%, respectively). The *EGFP* gene was also measured in the prostate of TRAMP mice (range: 0.12–0.85%), at higher levels compared with those detected in other tissues, including the peritoneum and the lungs (Figure 2A). These findings indicate that the prostate of TRAMP mice is also directly targeted by the lentiviral vector, albeit at low levels compared with the liver and the spleen, organs that conceivably represent the major source of transgene expression.

We then injected 6-weeks-old TRAMP mice with LV-IFN and analyzed transgene expression. Expression levels of the IFN-α-inducible interferon response factor (IRF)-7 gene, a sensitive indicator of IFN-α expression in murine models (28), were significantly upregulated (4- to 12-fold increase) in peripheral blood mononuclear cells from IFN-α-treated mice compared with expression values measured in control mice, upto 14 weeks after vector injection (Figure 2B). In agreement with previous studies utilizing this lentiviral vector (23), systemic IFN-α levels were very low (<12.5 pg/ml) and no IFN-α-related toxicity was observed.

We then killed the mice at serial time points and analyzed expression of a panel of IFN-α-inducible genes previously identified by microarray analysis of the IFN-α signature in EC (9). As shown in Figure 2C, sustained upregulation of IRF-7, IFIT-1, IFI27, Mx1–2, IFI204, CXCL10–11, GBP-1 and TNF-related apoptosis-inducing ligand transcripts was measured in the prostate of IFN-treated mice compared with controls at early time points of analysis. The expression of all these transcripts except IFI204 and Mx1–2 progressively decreased by 14 weeks after vector injection. VEGF levels were not substantially modified by IFN-α, whereas bFGF transcripts were slightly but significantly reduced at 14 weeks after vector injection compared with control TRAMP mice (Figure 2C). To study the effects of IFN-α at protein level, sections of the prostate were stained with antibodies to IFI204 or to Mx, two IFN-inducible genes that were upregulated in the prostate of IFN-α-treated mice (Figure 2C); results indicated a clear-cut difference in the intensity of IFI204 or Mx reactivity between IFN-treated and control mice (Figure 2D), confirming the results from RNA analysis.

IFN-α gene transfer impairs angiogenesis and proliferation in tumors

The upregulation of the angiostatic chemokines CXCL10 and CXCL11 along with the slight reduction in bFGF transcript levels hinted at a possible effect of IFN-α on angiogenesis. To investigate this, we performed staining with anti-CD31 of prostate sections obtained 14 weeks after LV-IFN injection and calculated the intraductal microvessel density. The intraductal capillary density in tumors of treated mice was reduced to 50% of that seen in control tumors (Figure 3A), indicating that treatment was attenuating the rate of neovascularization, albeit it did not completely block the initial activation of angiogenesis. Moreover, evaluation of pericyte coverage by staining with anti-NG2 Ab disclosed a significant difference between IFN-α-treated and control animals (Figure 3B); the percentage of pericyte coverage in IFN-α-treated TRAMP mice was higher than in controls and similar to values found in non-transgenic age-matched C57BL/6 mice, thus indicating that IFN-α was promoting vessel maturation. Notably, expression of angiopoietin 1, an angiogenic factor promoting vessel remodeling (29), was significantly increased in the prostate of IFN-α-treated animals (Figure 3B), and it could contribute to vessel normalization by this cytokine. Finally, most blood vessels in these initial phase of tumorigenesis were perfused and IFN-α treatment did not change these values (Figure 3C); in line with these findings, hypoxic areas were <5% in tumors from all groups, as evaluated by pimonidazole staining (data not shown).

These antiangiogenic effects were accompanied by a dramatic reduction in proliferation of the epithelial prostatic cells, as evaluated following staining with anti-Ki67 Ab (Figure 4A). Reduction of Ki67 staining was first noticed 3 weeks after LV-IFN administration and persisted up to 14 weeks thereafter (Figure 4A). In contrast, the total surface of areas of PIN or well-differentiated carcinoma were similar in IFN-α-treated or control mice (40.9 ± 28.7 and 46.8 ± 28.1, respectively). Apoptotic cells were detected following staining with anti-caspase 3 mAb, but their numbers were low and comparable between IFN-α-treated and control tumors (Figure 4B). Interestingly, expression levels of cyclin D2, a regulator of the cell cycle involved in prostate cancer progression (30), were significantly reduced in IFN-α-treated mice compared with controls (Figure 4C) and this was accompanied by concomitant upregulation of p16 expression, a key regulator of cyclin D2 (31). Altogether, these findings indicate that cyclin D2 and p16 could in part mediate IFN-α antiproliferative effects in this model.

Expression of IFN-α-regulated proteins in human prostatic cancer

In view of the marked biological effects exerted by IFN-α in the TRAMP model, we sought to investigate whether human prostatic cancer might show expression of endogenous IFN-α. To this end, we considered that hGBP-1 is among the most abundant cellular proteins expressed in IFN-treated cells (32). Since murine GBP-1 transcript levels were increased in the prostate of TRAMP treated with IFN-α, GBP-1 seemed to represent a suitable surrogate biomarker to investigate endogenous IFN-α expression in human samples. By using a mAb to hGBP-1, we found various patterns of hGBP-1 expression in 13 of 31 prostatic cancer samples analyzed (Figure 5A and Table I). Intriguingly, hGBP-1$^+$ tumor cells were found in seven samples and focal stromal reactivity, involving ECs or infiltrating leucocytes, was detected in further six samples (Figure 5A and Table I). In some samples, also basal cells of some normal prostatic glands showed hGBP-1 reactivity in the absence of inflammation (Figure 5A). There was not any obvious correlation between hGBP-1 expression and Gleason score, total prostate-specific antigen values, clinical or surgical stage of the samples (Table I). MxA, another IFN-α-regulated protein, was found expressed in 10 of 13 GBP-1$^+$ samples and in four of 10 GBP-1$^-$ samples. The overall good correlation between GBP-1 and MxA expression may indicate that endogenous IFN-α could drive expression of these IFN-inducible proteins.

Discussion

Here, we describe the biological effects of IFN-α during the early steps of prostate cancer progression. Our results strengthen the conclusions of previous studies, which have investigated this issue in models of liver adenocarcinoma (33) and of pancreatic cancer (16). Importantly, we observed that inhibition of angiogenesis represents a hallmark of IFN-α activity in the TRAMP model. This was primarily shown by marked reduction of the microvasculature in the prostate of IFN-α-treated mice compared with controls and by an improvement in the levels of pericyte coverage of microvessels. This finding may

TRAMP mice injected with the control vector were used as control (red line). (**D**) Immunofluorescence analysis of MxA and IFI204 expression in the prostate of TRAMP mice. One week after LV-IFN injection, sections of treated prostates were stained with an anti-MxA or anti-IFI204 (green) antibody followed by confocal microscopy analysis. Original magnification: ×200.

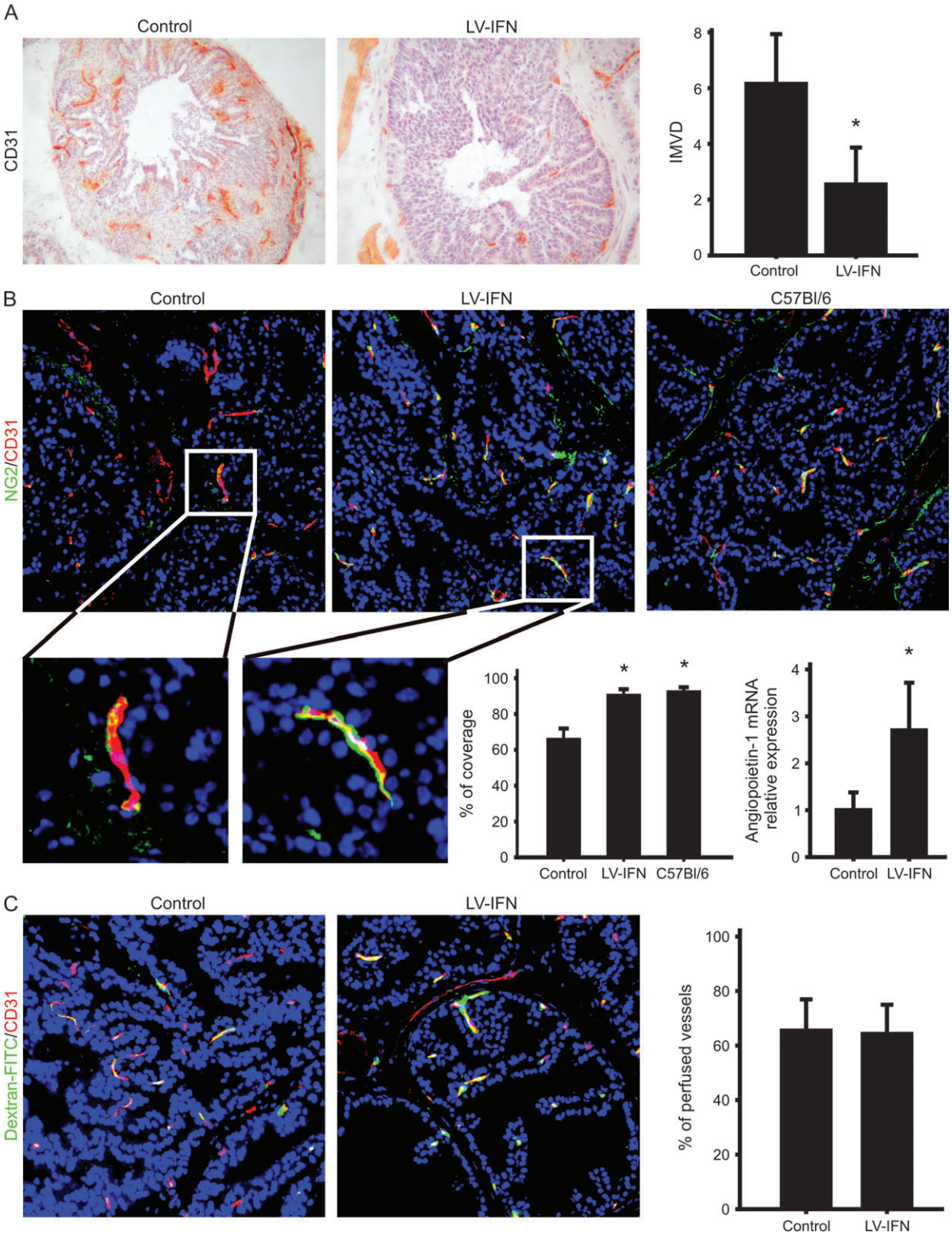

Fig. 3. Antiangiogenic effects following IFN-α gene transfer in TRAMP tumors. (**A**) Reduction of the IMVD in IFN-α-treated TRAMP tumors. Groups of 6-weeks-old TRAMP mice ($n = 12$) were injected with LV-IFN or the control vector. After 14 weeks, cryostatic sections of prostates were evaluated by CD31 immunohistochemistry and the IMVD was calculated. (**B**) Improvement of pericyte coverage in IFN-α-treated TRAMP mice. Tumor sections obtained 14 weeks after vector injection were stained with anti-NG2 (green) and anti-CD31 (red) antibodies, followed by immunofluorescence analysis. Top panels, representative images showing the different patterns of NG2 and CD31 staining in TRAMP tumors treated with LV-IFN or the control vector and in a prostate obtained from NT mouse (original magnification: ×200). Inset, ×400 magnification of selected vessels. Bottom panels: Left, quantitative analysis of vessel maturation following NG2 and CD31 staining ($n = 6$ samples per group). Right, measurement of angiopoietin 1 levels by quantitative PCR in TRAMP tumors ($n = 5$ samples per group). Mean ± SD is shown; $^{*}P < 0.05$. (**C**) Analysis of perfusion in IFN-α-treated compared with control tumors. Left panel, blood vessels were visualized by anti-CD31 staining (red); perfused vessels were identified by Dextran 70-fluorescein isothiocyanate (FITC) (green). Original magnification: ×200. Right panel, quantification of microvessel perfusion ($n = 6$ samples per group).

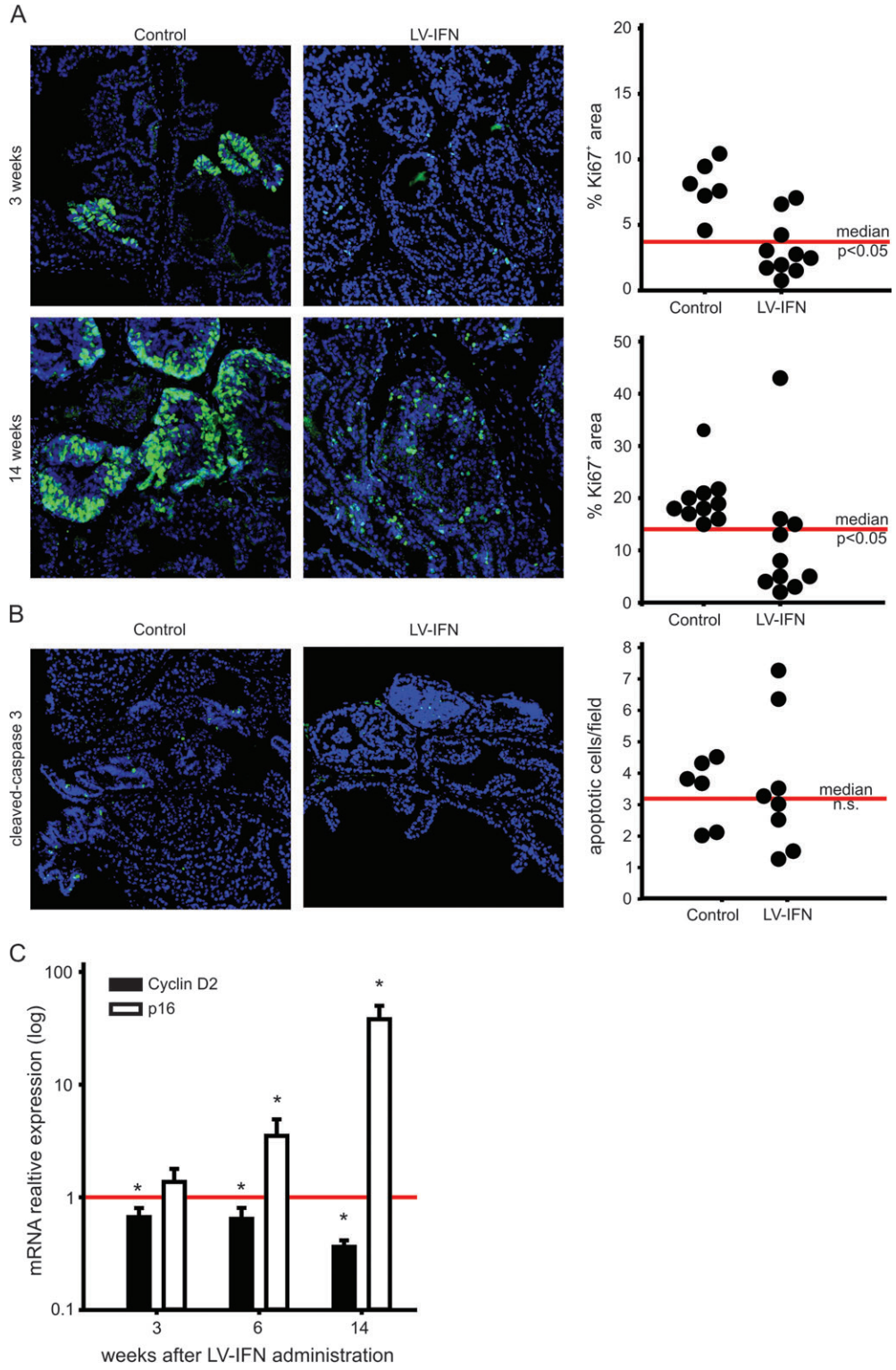

Fig. 4. Effects of IFN-α gene transfer on proliferation and apoptosis in TRAMP tumors. (**A**) Analysis of cell proliferation by Ki67 staining. Left panels, representative sections of early stage (3–6 weeks after treatment) or long term (14 weeks after treatment)-treated prostates incubated with an anti-Ki67 antibody (green). Original magnification: ×200. Right panels, quantitative analysis of Ki67$^+$ cells (n = 6–10 samples per group). (**B**) Analysis of apoptosis by activated caspase-3 staining. Left panel, representative sections of prostates (14 weeks after treatment) were incubated with an anti-cleaved-caspase 3 antibody (green). Original magnification: ×200. Right panels, quantitative analysis of caspase 3$^+$ cells (n = 6–8 samples per group); n.s., not significant. (**C**) Expression levels of cyclin D2 and p16 transcripts in prostates 3, 6 and 14 weeks after LV-IFN treatment. Prostates from TRAMP mice injected with the control vector were used as control (red line). Mean ± SD is shown. $^*P < 0.05$.

indicate that IFN-α supports vessel maturation, a novel activity of class I IFNs on the vasculature recently reported in xenograft tumor models (34,35). Previously, IFN-α/β was used in the RIP-Tag pancreatic tumor model with the intent to prevent the angiogenic switch, albeit in combination with other angiogenesis inhibitors (36) and antiangiogenic effects were similar to those reported here.

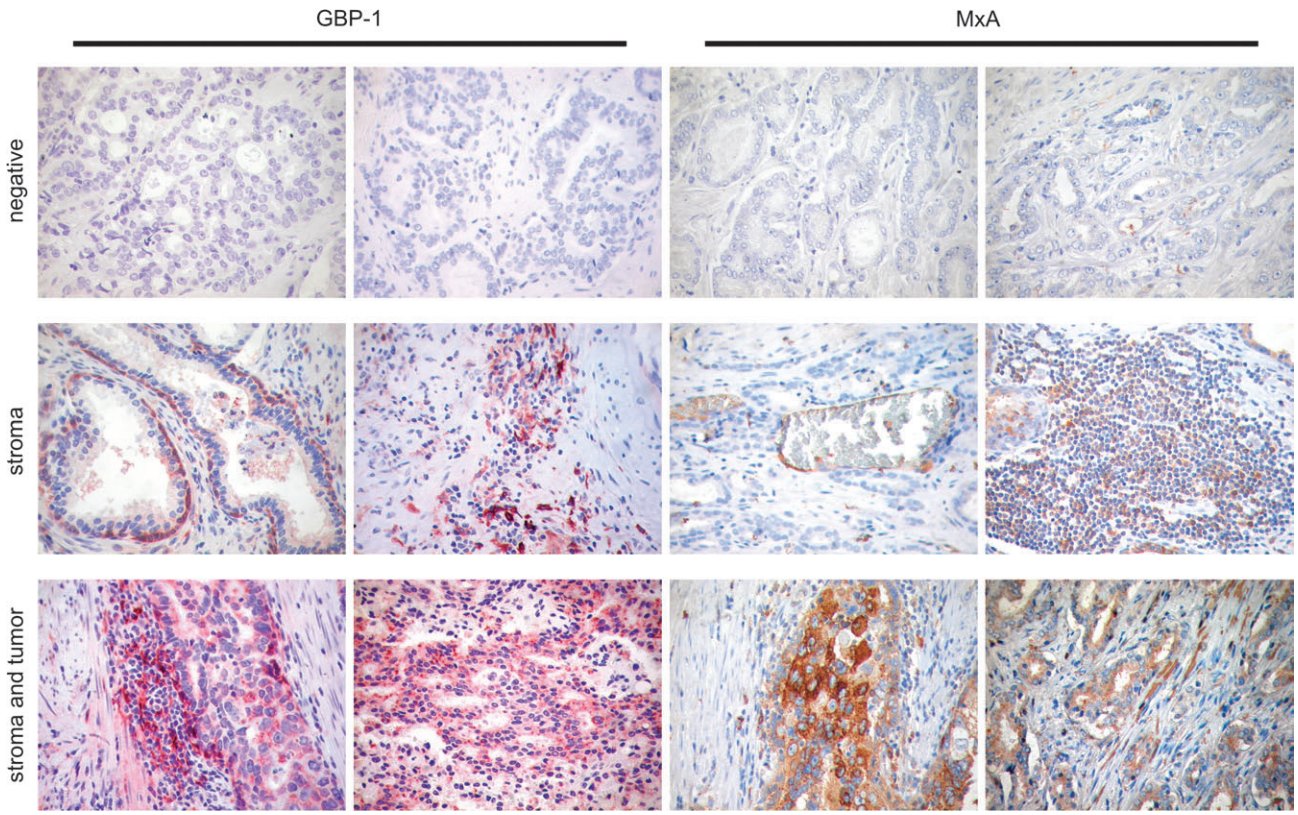

Fig. 5. Patterns of GBP-1 expression in human prostatic cancer. Representative patterns of GBP-1, MxA and CD34 staining in human prostatic cancer samples by immunohistochemistry. GBP1$^+$ or MxA$^+$ cells were found either in the stroma (including ECs, basal cells or inflammatory cells) or in the tumor. Two samples negative for GBP-1 staining are also shown. Original magnification: ×400.

How was the antiangiogenic effect generated? The angiogenic switch in the TRAMP model has previously been attributed mainly to VEGF (16), whose levels were, however, not affected by IFN-α (see Figure 1C). Interestingly, a significant reduction in bFGF transcript levels was measured in the prostate of treated animals, albeit only 14 weeks after treatment. Previous studies have shown that bFGF can also contribute to the angiogenic switch, as indicated by expression of bFGF both in PIN lesions and in advanced tumors (37). Moreover, genetic inactivation of one bFGF allele resulted in increased survival of TRAMP mice (38). Therefore, reduced bFGF levels could in part explain the antiangiogenic effect observed, although we cannot rule out that they could be secondary to reduction of the tumor mass, as they were detected at late time points after IFN-α administration.

Interestingly, transcriptional analysis of prostatic samples from IFN-α-treated TRAMP mice disclosed marked upregulation of several negative regulators of angiogenesis, including the angiostatic chemokines CXCL10-11 and GBP-1. Since the levels of these transcripts increased at early time points following treatment, they could mediate some of the vascular effects of IFN-α.

Besides these antiangiogenic effects, the other striking effect of IFN-α in our study was reduction of PIN cell proliferation. Upmodulation of genes endowed with antiproliferative functions, including IFI204 and p16, along with downregulation of cyclin D2 levels, may indicate that IFN-α directly inhibits PIN cell proliferation. IFI204, a member of the IFI family, encodes for a 72 kDa phosphoprotein involved in the control of growth and differentiation, primarily by binding and modulating the activity of transcription factors or their regulators, such as the retinoblastoma tumor suppressor protein (39). Moreover, p16 is a component of p16INK4A-Cdk4–6/cyclin D-retinoblastoma tumor suppressor protein-signaling pathways, which specifically binds to and inactivates CDK4/6, resulting in inactivation of CDK2 (40). Notably, p21, often involved as modulator of IFN-α or IFN-γ antiproliferative effects in prostatic cancer cells (41), had only marginal changes in this model (data not shown). These events eventually prevent phosphorylation of retinoblastoma tumor suppressor protein, leading to a stable cell cycle arrest. Nevertheless, evaluation of the antiproliferative effect of IFN-α *in vitro* on a panel of six TRAMP-derived tumor cell lines indicated minimal inhibition of cell proliferation (data not shown), thus suggesting that indirect antiproliferative effects could be at hand. Indirect proliferation control mechanisms could be mediated by stromal cells, including fibroblasts or EC. Indeed, physiological angiogenesis has been implied in the control of tissue mass in the normal prostate (42) and it is known that tumor-associated fibroblasts can modulate the tumorigenic potential of prostate epithelial cells (43). In any case, as the role of stromal cells in the control of tumor cell proliferation in the TRAMP model is unknown, this hypothesis remains speculative.

Class I IFNs have an established role in regulating the innate and adaptive arms of the immune system. Indeed, type I IFNs activate dendritic cells, upregulate the expression of major histocomptability complex class I molecules, promote the priming and survival of T cells, enhance humoral immunity and increase the cytotoxic activities of natural killer cells and CD8$^+$ T cells (44). In the TRAMP model, natural killer activity was increased in splenocytes from IFN-α-treated TRAMP mice (not shown), albeit we did not observe increased lymphocyte infiltration—including CD4$^+$, CD8$^+$ or natural killer cells—in IFN-α-treated prostates compared with controls (data not shown). Thus, immune-mediated mechanisms are not probably to contribute significantly to the reduction of cell proliferation and the antiangiogenic effects observed in preinvasive lesions.

To investigate the clinical relevance of our findings, we looked at the possible expression of IFN-inducible proteins (GBP-1 and MxA) in human samples of prostatic cancer. Limited information was available concerning GBP-1 expression in human cancer (45), although it is well recognized that GBP-1 expression is increased in areas of inflammation, which are often encountered in tumors (25,46,47). In

our series, we confirmed this but also found GBP-1 expressed in areas without apparent signs of inflammation, including GBP-1$^+$ tumor epithelial cells and basal cells in normal glandular structures. Previously, GBP-1 expression *in vivo* was almost exclusively associated with EC, where it may exert a specific function in response to class I IFNs and other inflammatory cytokines (25,47–49).

Whether GBP-1 expression in prostatic cancer is driven by endogenous IFN-α is currently unknown. In any case, the finding that ∼70% of the GBP-1$^+$ samples coexpressed MxA protein, suggests that their expression could be induced by endogenous IFN-α. Moreover, analysis of microarray data from public sources (50) indicated coordinated expression of GBP-1 and other IFN-α-regulated genes in prostatic cancer (data not shown), thus supporting this hypothesis. Intriguingly, a similar phenomenon has recently been observed in ∼32% of colorectal cancer samples (45) and this has been attributed to a Th-1-like immune response to tumor antigens. The limited number of samples analyzed in our study did not allow to draw any conclusion about the impact of the IFN signature on survival. In any case, assessment of expression of IFN-α-regulated genes by immunohistochemical analysis, as we have done here, will allow to conduct analysis of larger sample sets and this will help to ascertain the prognostic relevance of the IFN signature in prostatic cancer.

Finally, the description of the biological effects of IFN-α in the TRAMP model may have translational implications. In fact, about one-quarter of all prostate cancers occurs in family clusters and ∼9% can be attributed to hereditary prostate cancer with linkage to several prostate cancer susceptibility loci (51). Since the angiogenic switch has also been identified in human PIN (18), as well as in other preinvasive lesions (19), the recognition that this event can be contrasted by IFN-α will contribute to the development of prophylactic therapies based on IFN-α or other antiangiogenic drugs in high-risk individuals.

Supplementary material

Supplementary Table I can be found at http://carcin.oxfordjournals.org/

Funding

Associazione Italiana per la Ricerca sul Cancro (A.A.); Fondazione Italiana per la Ricerca sul Cancro (A.A.); Ministry of University and Research and Programmi di Ricerca di Rilevante Interesse Nazionale (A.A.); Ministry of Health, Oncology Program, grant no. RF-IOV-2006-408212 (A.A., S.I., U.P.); Banco Popolare di Verona (S.I.); Compagnia San Paolo di Torino (U.P.); Interdisciplinary Center for Clinical Research, University of Erlangen-Nuremberg (M.S. and E.N.).

Acknowledgements

We are grateful to Prof Santo Landolfo (University of Turin, Turin, Italy) for providing the anti-IFI204 antibody and for fruitful discussions, to Prof Otto Haller (University of Freiburg, Freiburg, Germany) for providing the anti-MxA antibody, to Vincenza Guzzardo (Pathology Unit, Azienda Ospedaliera, Padova) for technical assistance and to Ms Colette Case for help in the preparation of the manuscript.

Conflict of Interest Statement: None declared.

References

1. Minuzzo,S. *et al*. (2007) Angiogenesis meets immunology: cytokine gene therapy of cancer. *Mol. Aspects Med.*, **28**, 59–86.
2. Sidky,Y.A. *et al*. (1987) Inhibition of angiogenesis by interferons: effects on tumor- and lymphocyte-induced vascular responses. *Cancer Res.*, **47**, 5155–5161.
3. Rozera,C. *et al*. (1999) Interferon (IFN)-beta gene transfer into TS/A adenocarcinoma cells and comparison with IFN-alpha: differential effects on tumorigenicity and host response. *Am. J. Pathol.*, **154**, 1211–1222.
4. Indraccolo,S. *et al*. (2002) Differential effects of angiostatin, endostatin and interferon-alpha(1) gene transfer on *in vivo* growth of human breast cancer cells. *Gene Ther.*, **9**, 867–878.
5. Albini,A. *et al*. (2000) Inhibition of angiogenesis and vascular tumor growth by interferon-producing cells: a gene therapy approach. *Am. J. Pathol.*, **156**, 1381–1393.
6. Singh,R.K. *et al*. (1995) Interferons alpha and beta down-regulate the expression of basic fibroblast growth factor in human carcinomas. *Proc. Natl Acad. Sci. USA*, **92**, 4562–4566.
7. von Marschall,Z. *et al*. (2003) Effects of interferon alpha on vascular endothelial growth factor gene transcription and tumor angiogenesis. *J. Natl Cancer Inst.*, **95**, 437–448.
8. Oliveira,I.C. *et al*. (1992) Downregulation of interleukin 8 gene expression in human fibroblasts: unique mechanism of transcriptional inhibition by interferon. *Proc. Natl Acad. Sci. USA*, **89**, 9049–9053.
9. Indraccolo,S. *et al*. (2007) Identification of genes selectively regulated by IFNs in endothelial cells. *J. Immunol.*, **178**, 1122–1135.
10. Huang,S.F. *et al*. (2002) Inhibition of growth and metastasis of orthotopic human prostate cancer in athymic mice by combination therapy with pegylated interferon-alpha-2b and docetaxel. *Cancer Res.*, **62**, 5720–5726.
11. Dong,Z. *et al*. (1999) Suppression of angiogenesis, tumorigenicity, and metastasis by human prostate cancer cells engineered to produce interferon-beta. *Cancer Res.*, **59**, 872–879.
12. Zhang,F. *et al*. (2002) Tumor-infiltrating macrophages are involved in suppressing growth and metastasis of human prostate cancer cells by INF-beta gene therapy in nude mice. *Clin. Cancer Res.*, **8**, 2942–2951.
13. Cao,G. *et al*. (2001) Adenovirus-mediated interferon-beta gene therapy suppresses growth and metastasis of human prostate cancer in nude mice. *Cancer Gene Ther.*, **8**, 497–505.
14. Royuela,M. *et al*. (2000) Interferon-gamma and its functional receptors overexpression in benign prostatic hyperplasia and prostatic carcinoma: parallelism with c-myc and p53 expression. *Eur. Cytokine Netw.*, **11**, 119–127.
15. Greenberg,N.M. *et al*. (1995) Prostate cancer in a transgenic mouse. *Proc. Natl Acad. Sci. USA*, **92**, 3439–3443.
16. Huss,W.J. *et al*. (2001) Angiogenesis and prostate cancer: identification of a molecular progression switch. *Cancer Res.*, **61**, 2736–2743.
17. Bergers,G. *et al*. (2003) Tumorigenesis and the angiogenic switch. *Nat. Rev. Cancer*, **3**, 401–410.
18. Pallares,J. *et al*. (2006) Study of microvessel density and the expression of the angiogenic factors VEGF, bFGF and the receptors Flt-1 and FLK-1 in benign, premalignant and malignant prostate tissues. *Histol. Histopathol.*, **21**, 857–865.
19. Viacava,P. *et al*. (2004) Angiogenesis and VEGF expression in pre-invasive lesions of the human breast. *J. Pathol.*, **204**, 140–146.
20. Becker,C.M. *et al*. (2002) Gene therapy of prostate cancer with the soluble vascular endothelial growth factor receptor Flk1. *Cancer Biol. Ther.*, **1**, 548–553.
21. Huss,W.J. *et al*. (2003) SU5416 selectively impairs angiogenesis to induce prostate cancer-specific apoptosis. *Mol. Cancer Ther.*, **2**, 611–616.
22. Isayeva,T. *et al*. (2007) Effects of sustained antiangiogenic therapy in multistage prostate cancer in TRAMP model. *Cancer Res.*, **67**, 5789–5797.
23. Indraccolo,S. *et al*. (2005) Interferon-alpha gene therapy by lentiviral vectors contrasts ovarian cancer growth through angiogenesis inhibition. *Hum. Gene Ther.*, **16**, 957–970.
24. Indraccolo,S. *et al*. (2002) Gene transfer in ovarian cancer cells: a comparison between retroviral and lentiviral vectors. *Cancer Res.*, **62**, 6099–6107.
25. Lubeseder-Martellato,C. *et al*. (2002) Guanylate-binding protein-1 expression is selectively induced by inflammatory cytokines and is an activation marker of endothelial cells during inflammatory diseases. *Am. J. Pathol.*, **161**, 1749–1759.
26. Flohr,F. *et al*. (1999) The central interactive region of human MxA GTPase is involved in GTPase activation and interaction with viral target structures. *FEBS Lett.*, **463**, 24–28.
27. Gariglio,M. *et al*. (1998) The murine homolog of the HIN 200 family, Ifi 204, is constitutively expressed in myeloid cells and selectively induced in the monocyte/macrophage lineage. *J. Leukoc. Biol.*, **64**, 608–614.
28. Indraccolo,S. *et al*. (2006) Gene therapy of ovarian cancer with IFN-alpha-producing fibroblasts: comparison of constitutive and inducible vectors. *Gene Ther.*, **13**, 953–965.
29. Jain,R.K. (2003) Molecular regulation of vessel maturation. *Nat. Med.*, **9**, 685–693.
30. Sun,A. *et al*. (2008) Androgen receptor-dependent regulation of Bcl-xL expression: implication in prostate cancer progression. *Prostate*, **68**, 453–461.

31. Busk,P.K. *et al*. (2005) Cyclin D2 induces proliferation of cardiac myocytes and represses hypertrophy. *Exp. Cell Res.*, **304**, 149–161.
32. Cheng,Y.S. *et al*. (1983) Interferon induction of fibroblast proteins with guanylate binding activity. *J. Biol. Chem.*, **258**, 7746–7750.
33. Nakaji,M. *et al*. (2004) IFN-alpha prevents the growth of pre-neoplastic lesions and inhibits the development of hepatocellular carcinoma in the rat. *Carcinogenesis*, **25**, 389–397.
34. De Palma,M. *et al*. (2008) Tumor-targeted interferon-alpha delivery by Tie2-expressing monocytes inhibits tumor growth and metastasis. *Cancer Cell*, **14**, 299–311.
35. Dickson,P.V. *et al*. (2007) Continuous delivery of IFN-beta promotes sustained maturation of intratumoral vasculature. *Mol. Cancer Res.*, **5**, 531–542.
36. Parangi,S. *et al*. (1996) Antiangiogenic therapy of transgenic mice impairs de novo tumor growth. *Proc. Natl Acad. Sci. USA*, **93**, 2002–2007.
37. Huss,W.J. *et al*. (2003) Differential expression of specific FGF ligand and receptor isoforms during angiogenesis associated with prostate cancer progression. *Prostate*, **54**, 8–16.
38. Polnaszek,N. *et al*. (2003) Fibroblast growth factor 2 promotes tumor progression in an autochthonous mouse model of prostate cancer. *Cancer Res.*, **63**, 5754–5760.
39. Asefa,B. *et al*. (2004) The interferon-inducible p200 family of proteins: a perspective on their roles in cell cycle regulation and differentiation. *Blood Cells Mol. Dis.*, **32**, 155–167.
40. Gil,J. *et al*. (2006) Regulation of the INK4b-ARF-INK4a tumour suppressor locus: all for one or one for all. *Nat. Rev. Mol. Cell Biol.*, **7**, 667–677.
41. Hobeika,A.C. *et al*. (1997) IFNalpha induces the expression of the cyclin-dependent kinase inhibitor p21 in human prostate cancer cells. *Oncogene*, **14**, 1165–1170.
42. Folkman,J. (1998) Is tissue mass regulated by vascular endothelial cells? Prostate as the first evidence. *Endocrinology*, **139**, 441–442.
43. Olumi,A.F. *et al*. (1999) Carcinoma-associated fibroblasts direct tumor progression of initiated human prostatic epithelium. *Cancer Res.*, **59**, 5002–5011.
44. Belardelli,F. *et al*. (2002) Interferon-alpha in tumor immunity and immunotherapy. *Cytokine Growth Factor Rev.*, **13**, 119–134.
45. Naschberger,E. *et al*. (2008) Angiostatic immune reaction in colorectal carcinoma: impact on survival and perspectives for antiangiogenic therapy. *Int. J. Cancer*, **123**, 2120–2129.
46. Naschberger,E. *et al*. (2006) Human guanylate binding protein-1 is a secreted GTPase present in increased concentrations in the cerebrospinal fluid of patients with bacterial meningitis. *Am. J. Pathol.*, **169**, 1088–1099.
47. Naschberger,E. *et al*. (2005) Human guanylate binding protein-1 (hGBP-1) characterizes and establishes a non-angiogenic endothelial cell activation phenotype in inflammatory diseases. *Adv. Enzyme Regul.*, **45**, 215–227.
48. Naschberger,E. *et al*. (2004) Nuclear factor-kappaB motif and interferon-alpha-stimulated response element co-operate in the activation of guanylate-binding protein-1 expression by inflammatory cytokines in endothelial cells. *Biochem. J.*, **379**, 409–420.
49. Guenzi,E. *et al*. (2003) The guanylate binding protein-1 GTPase controls the invasive and angiogenic capability of endothelial cells through inhibition of MMP-1 expression. *EMBO J.*, **22**, 3772–3782.
50. Varambally,S. *et al*. (2005) Integrative genomic and proteomic analysis of prostate cancer reveals signatures of metastatic progression. *Cancer Cell*, **8**, 393–406.
51. Shand,R.L. *et al*. (2006) Molecular biology of prostate-cancer pathogenesis. *Curr. Opin. Urol.*, **16**, 123–131.

Received October 21, 2008; revised February 3, 2009;
accepted February 4, 2009